Hydrogeology Journal (2019) 27:2637–2643
https://doi.org/10.1007/s10040-019-02010-2

PAPER

A continuum-scale two-parameter model for non-Darcian flow in low-permeability porous media

Cheng Chen[1]

Received: 28 October 2018 / Accepted: 20 June 2019 / Published online: 4 July 2019

Abstract
Numerous studies have demonstrated that Darcy velocity exhibits nonlinear dependence on the pressure gradient in lower-permeability porous media such as clays and shales when the pressure gradient is low. Non-Darcian flow has important implications to geologic disposal of high-level nuclear waste, because shale has been proposed as a disposal medium, with compacted bentonite clay as a buffer material. Consideration of the impact of temperature on non-Darcian flow in an engineered clay barrier is necessary, because the clay barrier is subjected to significant temperature changes resulting from the heat-releasing nuclear waste package. In this study, a continuum-scale, two-parameter predictive model is developed to facilitate experimental data interpretation and to provide mechanistic insights into the role of temperature on non-Darcian flow in saturated low-permeability porous media. This model has several advantages when it is applied at the continuum scale. First, this model is consistent with the current theory about the role of temperature and provides more flexibility in fitting experimental data associated with varying temperatures. Second, the values of the two independent parameters in the model can be easily determined and the solution is unique. This leads to practical convenience when the model is used to interpret continuum-scale laboratory data. Third, although the two-parameter model is simple, its performance in fitting existing experimental data is satisfactory. This suggests that the model achieves a balance between simplicity and effectiveness.

Keywords Non-Darian flow · Groundwater flow · Conceptual model · Temperature · Threshold gradient

Introduction

Darcy's law, characterized by a linear correlation between flow velocity and pressure gradient, is widely used to describe fluid flow in porous media (Bear 1979; Chen et al. 2010) and is the basis of most reservoir simulators. However, numerous studies (Miller and Low 1963; Bear 1979; Hansbo 2001; Sanchez et al. 2007; Cui et al. 2008; Liu and Birkholzer 2012; Liu et al. 2012) have demonstrated that Darcy velocity, in both saturated and unsaturated flows, exhibits nonlinear dependence on the pressure gradient in low-permeability porous media such as clays and shales when the pressure gradient is low. Non-Darcian flow results from the strong liquid–solid interactions (Miller and Low 1963) in a thin layer close to clay surface, which are the combined effects of various interfacial forces including the van der Waals forces (Liu 2017). In low-permeability porous media, such as the shale formations and engineered clay barriers in nuclear waste repositories, the nanoscale pore size is comparable to the interfacial layer thickness so the influence of strong liquid-solid interactions is not negligible (Wang 2014; Chen 2016). A certain hydraulic gradient (i.e., the threshold gradient) is required to overcome the binding energy between water molecules and solid surfaces to trigger water flow (Miller and Low 1963; Hansbo 2001), which leads to a nonlinear relationship between water flux and pressure gradient (Liu et al. 2016).

Non-Darcian flow has important implications to geologic disposal of high-level nuclear waste, because shale has been proposed as a disposal medium with compacted bentonite clay as a buffer material. Non-Darcian flow can occur in both the geologic barrier (shale) and engineered barrier (bentonite clay) systems (Liu 2014). For example, non-Darcian flow can lead to extremely low water velocity in the excavation damaged zone (EDZ) of a shale host rock, much lower than the velocity predicted by a Darcian flow model, and as a result diffusion will dominate solute transport in the EDZ (Bianchi et al.

✉ Cheng Chen
chen08@vt.edu

[1] Department of Mining and Minerals Engineering, Virginia Tech, Blacksburg, VA, USA

2015). In a bentonite clay buffer, the initial water content is usually low, which causes water imbibition into the buffer from the surrounding host rock (Rutqvist et al. 2011). This process develops an unsaturated zone in the near field of the waste container. Water flow under unsaturated conditions in bentonite clay usually shows stronger non-Darcian behaviors than saturated conditions, because in unsaturated media water generally occupies smaller pores and has lower connectivity (Liu et al. 2012; Fan et al. 2018). Advanced understanding of non-Darcian flow in a bentonite clay buffer is critical for accurate prediction of water migration and saturation evolution over the time scale of 100,000 years in the near field of a repository. Heat generated by nuclear waste will greatly affect the distribution and transfer of water in the bentonite clay buffer. Furthermore, the wetting process resulting from water imbibition causes the bentonite clay to swell, which increases in-situ stress and provides an improved sealing effect to close the open space between the waste container and host formation. Thus, advanced understanding of non-Darcian flows in engineered clay barriers is crucial to accurately simulate the coupled thermal-hydrological-mechanical (THM) processes (Rutqvist et al. 2011, 2014) and to reduce uncertainties associated with long-term performance assessment of nuclear waste disposal. Furthermore, study of non-Darcian flow in low-permeability media has direct applications to the recovery of unconventional hydrocarbon resources such as shale oil and gas, which requires improved understanding of the flow and transport processes in low-permeability shale formations (Chen 2016).

Consideration of the impact of temperature on non-Darcian flow in an engineered clay barrier is necessary, because the clay barrier is subjected to significant temperature changes resulting from the heat-releasing nuclear waste package. For instance, a recent THM simulation (Rutqvist et al. 2011) indicated that the temperature evolution in a bentonite-backfilled engineered barrier could be from a level lower than 30 °C to around 90 °C over a time scale of 100,000 years. The temperature can be even higher depending on the configuration of waste emplacement. Although experimental data with respect to the role of temperature on non-Darcian flows are rare, at least two groups (Miller and Low 1963; Zeng et al. 2010) reported inspiring experimental data. Miller and Low (1963) defined threshold gradient as the pressure gradient below which no flow occurs. They measured threshold gradient in a clay sample under two temperatures (10.15 and 20.00 °C) and found that it decreased with increased temperature; they speculated that the increased temperature might weaken the binding energy between water molecules and clay surfaces. Zeng et al. (2010) measured the threshold gradient for oil flow in low-permeability sandstones under two temperatures (70 and 90 °C) and found a similar conclusion as Miller and Low (1963). Although these experimental results are remarkable, an advanced theoretical framework is needed to improve the fundamental understanding of the temperature dependence of non-Darcian flow in low-permeability porous media.

In this study, a continuum-scale, two-parameter predictive model is developed to facilitate experimental data interpretation and to provide mechanistic insights into the role of temperature on non-Darcian flow in saturated low-permeability porous media. Specifically, the new theoretical and modeling framework, when calibrated with experimental data, has the potential to improve the fundamental understanding of the temperature dependence of the threshold gradient in saturated non-Darcian flow and thus can provide reliable model inputs for coupled THM simulations for bentonite clay buffers in nuclear waste repositories.

Methods

Threshold and critical hydraulic gradients

In this study, the threshold gradient (J_t) is defined as the gradient below which no flow occurs. The critical gradient (J_c) is the intersection between the x (gradient) axis and the extension of the linear part of the curve, as shown in Fig. 1. The definition of threshold gradient (J_t) used here is the same as those in experimental studies such as Miller and Low (1963), Zeng et al. (2010), and Sanchez et al. (2007). This is because J_t is straightforward and convenient to capture in experiments if equipment accuracy is sufficiently high. Conversely, Liu (2014) defined J_c in Fig. 1 as the threshold gradient. Generally, from a modeling perspective, defining J_c as the threshold gradient will bring certain convenience in establishing the nonlinear relationship between water flux and gradient. For example, Liu and Birkholzer (2012) developed a three-parameter, generalized Darcy's law, which under certain circumstances reduces to the correlations of Bear (1979) ($J_t = J_c > 0$), Swartzendruber (1961) ($J_t = 0$ and $J_c > 0$), and classic Darcy's law ($J_t = J_c = 0$).

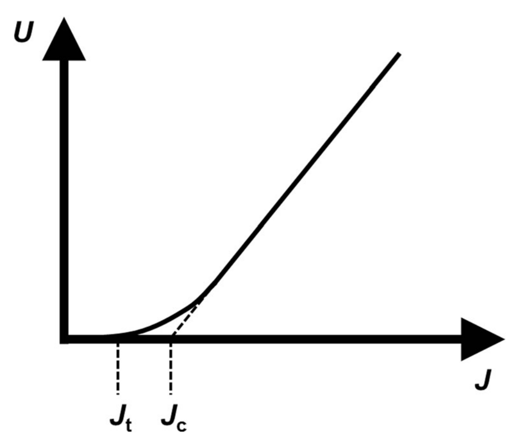

Fig. 1 Threshold gradient (J_t) and critical gradient (J_c) in non-Darcian flow. U is flow velocity and J is hydraulic gradient

Conceptual model

It is hypothesized that there is an "effective" immobile layer at the liquid-solid interface in nanotube flow. This effective immobile layer is an ensemble concept, which takes into account all combined effects that hinder fluid movement in low-permeability porous media such as strong liquid-solid interactions at solid surfaces, pore size heterogeneity, and barrier energy required for the fluid to enter small hydrophobic pores. It is hypothesized that the thickness of this immobile layer (h) decreases exponentially as the velocity gradient at the tube wall increases:

$$h = h_0 \exp\left(-a \frac{\partial u}{\partial r}\bigg|_{r=R}\right) \quad (1)$$

where r is the distance from the tube center (m), R is tube radius (m), h_0 is the initial immobile layer thickness (m) when the flow velocity is zero, and a is the characteristic time (s). Both parameters (h_0 and a) are positive, might depend on the temperature, and need to be determined by fitting experimental data, which will be discussed later. It should be noted that Eq. (1) is formulated to enhance the two-parameter model's capability in fitting the phenomenological correlation between threshold gradient and clay permeability at the laboratory scale. For incompressible Newtonian laminar flow in a circular tube (Gerhart and Gross 1990), one has:

$$\frac{\partial u}{\partial r}\bigg|_{r=R} = \frac{R}{2\mu}\left|\frac{\partial p}{\partial x}\right| \quad (2)$$

where μ is water viscosity (Pa s), and $\partial p/\partial x$ is pressure gradient (Pa/m). Plugging Eq. (2) into Eq. (1), one obtains:

$$h = h_0 \exp\left(-\frac{aR}{2\mu}\left|\frac{\partial p}{\partial x}\right|\right) \quad (3)$$

The apparent permeability (Chen 2016) (k_a) which is subjected to the influence of the effective immobile layer, is calculated as:

$$k_a = \frac{1}{8}(R-h)^2 \quad (4)$$

Combining Eqs. (3) with (4), one obtains:

$$k_a = \frac{1}{8}\left[R - h_0 \exp\left(-\frac{aR}{2\mu}\left|\frac{\partial p}{\partial x}\right|\right)\right]^2 \quad (5)$$

When h is sufficiently low due to the increased pressure gradient, $R \geq h$, which suggests that water flow starts to occur. One can calculate the threshold pressure gradient, J_t (Pa/m), which is the minimum absolute value of $\partial p/\partial x$ needed to ensure a positive value inside the parentheses on the right-hand side of Eq. (5):

$$J_t = \begin{cases} \left(\frac{-2\mu}{aR}\right)\ln\left(\frac{R}{h_0}\right) & \text{if } h_0 > R \\ 0 & \text{if } h_0 \leq R \end{cases} \quad (6)$$

Results

Fitting experimental data

The threshold gradient as a function of permeability based on Eq. (6) is plotted, as illustrated in Fig. 2. Specifically, given the effective pore radius (R) the absolute permeability of the porous medium is calculated as $k = R^2/8$ and plotted as the x axis. R is then used to calculate the threshold gradient based on Eq. (6) and plotted as the y axis. It is assumed that $\mu = 0.001$ Pa s (water viscosity at the temperature of 20 °C), $a = 1$ s, and $h_0 = 1$ µm, which is larger than all R values used in Fig. 2 so a non-zero threshold gradient is needed to initiate fluid flow (see Eq. 6). With the two parameters (a and h_0) determined tentatively, this base scenario (scenario 1) shows a power-law relationship between the threshold gradient, J_t (m/m), and the permeability, k (m^2):

$$J_t = 9 \times 10^{-13} k^{-0.85} \quad (7)$$

Liu and Birkholzer (2012) also found a power-law correlation (Fig. 3) between J_t (m/m) and k (m^2) by fitting experimental data from seven groups (Lutz and Kemper 1959; Miller and Low 1963; Blecker 1970; Dubin and Moulin 1986; Zou 1996; Cui et al. 2008; Wang et al. 2011):

$$J_t = A k^B \quad (8)$$

where $A = 4.0 \times 10^{-12}$ and $B = -0.78$. Note that in this two-parameter model $a = 1$ s and $h_0 = 1$ µm were chosen as the initial, tentative parameter values. The values of a and h_0 will then be adjusted to match the values of A and B which result from experimental data fitting. By investigating Eq. (6), it is found that changing the value of h_0 will change both A and B. Conversely, changing the value of a will only change A. In other words, when the temperature is fixed (i.e., fixed μ), the coefficient (A) depends on both a and h_0, whereas the power-law exponent (B) depends only on h_0. This suggests that, although there are two unknown parameters (a and h_0) in Eq. (6), it is possible to find a unique solution to them by fitting experimental data. Specific workflow is as follows:

Step 1: Conduct laboratory experiments and then use data fitting to obtain the empirical, power-law correlation between threshold gradient and medium permeability, $J_t = Ak^B$.

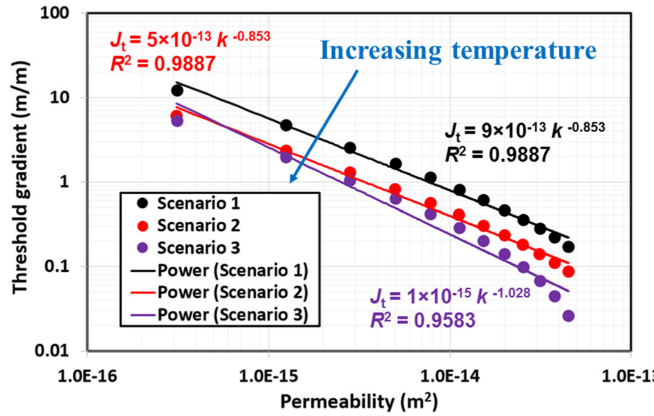

Fig. 2 Threshold gradient (J_t) as a function of permeability (k) based on Eq. (6). Temperatures in scenarios 1 and 2 are 20 °C and 55 °C, respectively. In scenario 3, temperature is still 55 °C but h_0 is reduced to 0.7 μm

Step 2: Fit the experimental data using Eq. (6); adjust the value of h_0 to match the power-law exponent (B).

Step 3: Adjust the value of a to match the coefficient (A).

Using this workflow, it is found that $h_0 = 1.4$ μm and $a = 4$ s, which lead to $A = 4.0 \times 10^{-12}$ and $B = -0.78$, exactly the same as the coefficients found by Liu and Birkholzer (2012) for Eq. (8). Therefore, it is clear that the continuum-scale two-parameter model is able to fit experimental data, and unique values of the two parameters (a and h_0) can be determined in the data fitting process based on the workflow.

Sensitivity analysis and temperature dependence

The values of a and h_0 are then adjusted for sensitivity analysis, as illustrated in Fig. 2. Scenario 1 ($a = 1$ s and $h_0 = 1$ μm) is referred to as the base scenario. In scenario 2, it is assumed that temperature is raised to 55 °C so fluid viscosity accordingly drops to 0.0005 Pa s. It is observed that the curve for scenario 2 is shifted downward in a parallel manner, without any change in the power-law exponent (−0.85). In scenario 3, the value of h_0 is artificially reduced to 0.7 μm when the temperature is 55 °C, because it is hypothesized that the increased temperature leads to a thinner effective immobile layer. The resultant curve shows that the reduction of h_0 further shifts the curve downward and it has a more significant influence on higher permeabilities. As a consequence, scenario 3 shows a steeper slope in the log-log plot, leading to a higher absolute value of the power-law component (−1.03).

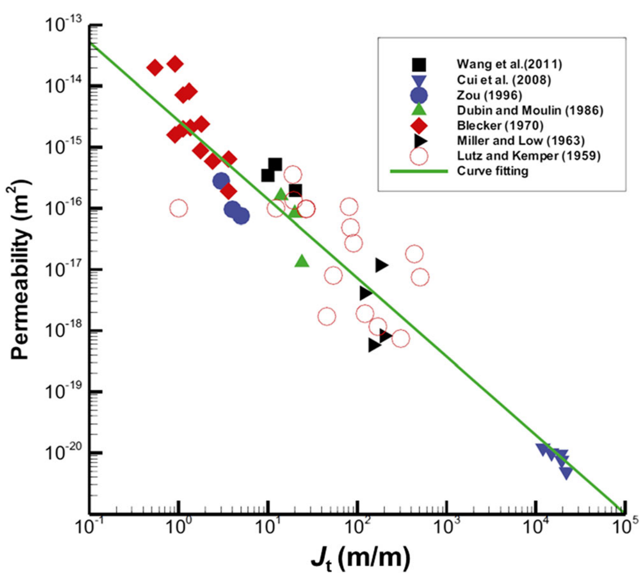

Fig. 3 Correlation between permeability (k) and threshold hydraulic gradient (J_t) by fitting experimental data from seven groups. Modified from Liu and Birkholzer (2012)

Based on Eq. (8) and the available experimental data in the literature (Miller and Low 1963; Zeng et al. 2010), Liu (2014) suggested an empirical correlation to account for the effect of temperature on the threshold gradient in saturated non-Darcian flow:

$$J_t = Ak^B(\mu_{ref}/\mu)^B \tag{9}$$

where μ_{ref} and μ are water viscosities at the reference temperature and current temperature, respectively. With a negative value of B, an increased temperature (i.e., reduced fluid viscosity) will result in a smaller J_t. Equation (9) suggests that temperature affects only fluid viscosity and is unable to influence the value of the power-law exponent (B). The temperature dependence of threshold gradient based on Eq. (9) is illustrated in Fig. 4, which illustrates the same trend as that described in scenario 2 in Fig. 2 (i.e., the threshold gradient-permeability correlation shifts in a parallel manner under the influence of the varying temperature). Furthermore, the proposed two-parameter framework is able to capture more complicated trends that involve the change of the power-law exponent (i.e., scenario 3 in Fig. 2). In this study, the two-parameter predictive model provides higher flexibility because of the two independent parameters (a and h_0). Adjusting μ and a changes A, while adjusting h_0 changes both A and B. All of these properties of Eq. (6), associated with the data-fitting workflow described in the preceding section

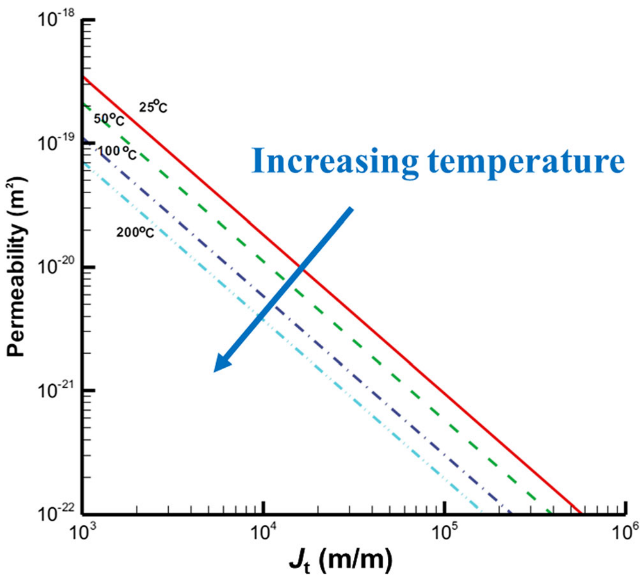

Fig. 4 Temperature dependence of threshold gradient based on Eq. (9). Modified from Liu (2014)

'Fitting experimental data', give the new model a lot of flexibility and physical insights in fitting experimental data associated with varying temperatures.

Table 1 summarizes the values of the two parameters, *a* and h_0, and the value of fluid viscosity, μ, in the continuum-scale predictive model (Eq. 6), as well as the corresponding values of the two fitting coefficients (*A* and *B*) in the empirical power-law correlation (Eq. 8). As described previously, in scenarios 1–3 illustrated in Fig. 2, the values of *a* and h_0 are assigned in Eq. (6) first, and then the generated data (J_t and *k*) are fitted using the power-law correlation to determine the values of *A* and *B*. The purpose of demonstrating scenarios 1–3 in Fig. 2 is to investigate the influence of the values of *a* and h_0 on the empirical power-law correlation. When fitting the experimental data shown in Fig. 3, however, the procedure is reverse. The values of *A* and *B* are determined first by fitting the empirical power-law correlation to the experimental data from the seven research groups shown in Fig. 3. The values of the two parameters, *a* and h_0, are then adjusted to match the determined values of *A* and *B* using the data fitting workflow described in the preceding section 'Fitting experimental data', and a unique solution to *a* and h_0 can be found.

Based on the parameter values in scenarios 1–3, Darcy's law, in which the permeability is calculated by Eq. (5), is used to plot apparent flow velocity (*U*) as a function of pressure gradient (*J*) in a clay sample having permeability of 3.13×10^{-16} m^2, as demonstrated in Fig. 5. The shape of the velocity-gradient curves is similar to that observed in laboratory experiments (Sanchez et al. 2007; Zeng et al. 2010), and the proposed two-parameter predictive model is able to capture both the threshold (J_t) and critical (J_c) gradients, as defined in Fig. 1. Reduced fluid viscosity resulting from increased temperature (scenario 2) leads to lower J_t and J_c, as well as higher linear-part slope due to the increased fluid mobility (i.e., k/μ), which is consistent with the experimental finding of Zeng et al. (2010). Figure 5 also shows that decreased h_0 (scenario 3) leads to lower J_t and J_c but does not cause significant changes in the linear-part slope. This implies that in future research it is critical to study the role of increased temperature on h_0 besides studying its role on fluid viscosity.

Discussion and conclusion

The continuum-scale, two-parameter predictive model developed in this study aims to interpret the phenomenological correlation between threshold gradient and clay permeability in saturated non-Darcian flow. This model has several advantages when it is applied at the continuum scale. First, sensitivity analyses demonstrate that this model is consistent with the current theory about the role of temperature on the threshold gradient (Eq. 9). The current theory is a pioneering work developed by Liu (2014) based on the analysis of available experimental data. It assumes that the temperature influences only fluid viscosity, and thus does not change the exponent value in the power law that describes the phenomenological correlation between threshold gradient and clay permeability. In the future, when more experimental data with respect to varying temperatures are available, there is a need to account for the variation in the power-law exponent due to the temperature change. Thus, the two-parameter modeling framework provides more flexibility and mechanistic insights in fitting experimental data associated with varying temperatures because of the two independent parameters in the model

Table 1 Values of the two parameters (*a* and h_0) the fluid viscosity (μ) and the two fitting coefficients (*A* and *B*) in scenarios 1–3 (Fig. 2) and the process of fitting experimental data (Fig. 3)

Parameter	Scenario 1	Scenario 2	Scenario 3	Fitting experimental data in Fig. 3
a (s)	1	1	1	4
h_0 (μm)	1	1	0.7	1.4
μ (Pa s)	1×10^{-3}	5×10^{-4}	5×10^{-4}	1×10^{-3}
A	9×10^{-13}	5×10^{-13}	1×10^{-15}	4×10^{-12}
B	−0.85	−0.85	−1.03	−0.78

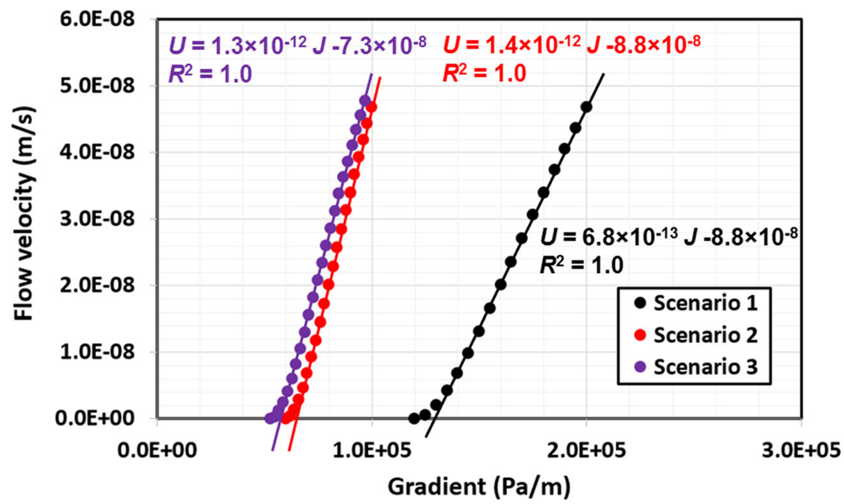

Fig. 5 Apparent flow velocity (U) as a function of pressure gradient (J) using Eq. (5) for the calculation of permeability in Darcy's law

(Fig. 2). Second, although the proposed model has two independent parameters, their values can be readily determined using the data-fitting workflow described in section 'Fitting experimental data', and the solution to the parameter values is unique. This leads to practical convenience and advantage when the two-parameter model is used to interpret continuum-scale laboratory data. Third, although the two-parameter model is simple, its performance in fitting experimental data is satisfactory. The model successfully fits existing experimental data collected by other research groups (Fig. 3). Moreover, the two-parameter model is able to accurately describe the nonlinear relationship between apparent flow velocity and hydraulic gradient (Fig. 5), which is consistent with experimental observations in the laboratory. This suggests that the two-parameter model achieves a balance between model simplicity and effectiveness.

The two-parameter modeling framework is developed at the continuum scale, and for the sake of simplicity it does not account for the pore-scale difference between interlayer space (micropores) and outerlayer space (macropores) in clays. This is because the current theory about the relationship between threshold gradient and clay permeability, which is based on an empirical, power-law correlation (Eq. 8), uses the overall clay permeability measured at the laboratory scale, which is contributed by both the micropores and macropores. Therefore, the continuum-scale, two-parameter model does not differentiate internal pores at the two spatial scales, and as a consequence the double-structure pore geometry framework (Sanchez et al. 2005) is not used in this model. The simplification of clay pore geometry in the two-parameter model leads to certain convenience in its practical application at the continuum scale, especially in fitting laboratory hydrodynamic experimental data. The new theoretical and modeling framework, when fitted with experimental data, can improve the fundamental understanding of the temperature dependence of the threshold gradient in saturated non-Darcian flow and provide reliable model inputs for coupled THM simulations for bentonite clay buffers in nuclear waste repositories.

Acknowledgements The author is thankful to Dr. Hui-Hai Liu, Dr. Yifeng Wang, Dr. Rui Qiao, and Dr. Liange Zheng for the helpful discussions.

Funding information The author gratefully acknowledges the support of the US Department of Energy's Nuclear Energy University Program through grant DE-NE0008806.

References

Bear J (1979) Hydraulics of groundwater. McGraw-Hill, New York

Bianchi M, Liu HH, Birkholzer JT (2015) Radionuclide transport behavior in a generic geological radioactive waste repository. Groundwater 53(3):440–451

Blecker RF (1970) Saturated flow of water through clay loam subsoil material of the Brolliat and Springerville soil series. MSc Thesis, University of Arizona, Tucson, AZ

Chen C (2016) Multiscale imaging, modeling, and principal component analysis of gas transport in shale reservoirs. Fuel 182:761–770

Chen C, Packman AI, Zhang DX, Gaillard JF (2010) A multi-scale investigation of interfacial transport, pore fluid flow, and fine particle deposition in a sediment bed. Water Resour Res 46, W11560

Cui YJ, Tang AM, Loiseau C, Delage P (2008) Determining the unsaturated hydraulic conductivity of a compacted sand-bentonite mixture under constant-volume and free-swell conditions. Phys Chem Earth 33:S462–S471

Dubin B, Moulin G (1986) Influences of critical gradient on the consolidation of clay. In: Young T (ed) Consolidation of soils, testing and evaluation. ASTM STP 892, West Conshohocken, PA, pp 354–377

Fan M, McClure J, Han Y, Chen C (2018) Interaction between proppant compaction and single−/multiphase flows in a hydraulic fracture. SPE J. https://doi.org/10.4043/27907-MS

Gerhart P, Gross R (1990) Fundamentals of fluid mechanics. Addison-Wesley, New York

Hansbo S (2001) Consolidation equation valid for both Darcian and non-Darcian flow. Geotechnique 51(1):51–54

Liu H (2017) Fluid flow in the subsurface: history, generalization and applications of physical Laws. Springer, Heidelberg, Germany

Liu HH (2014) Non-Darcian flow in low-permeability media: key issues related to geological disposal of high-level nuclear waste in shale formations. Hydrogeol J 22(7):1525–1534

Liu HH, Birkholzer J (2012) On the relationship between water flux and hydraulic gradient for unsaturated and saturated clay. J Hydrol 475: 242–247

Liu HH, Lai BT, Chen JH (2016) Unconventional spontaneous imbibition into shale matrix: theory and a methodology to determine relevant parameters. Transp Porous Media 111(1):41–57

Liu HH, Li LC, Birkholzer J (2012) Unsaturated properties for non-Darcian water flow in clay. J Hydrol 430:173–178

Lutz JF, Kemper WD (1959) Intrinsic permeability of clay as effected by clay–water interaction. Soil Sci 88:83–90

Miller R, Low P (1963) Threshold gradient for water flow in clay systems. Soil Sci Soc Am Proc 27(6):605–609

Rutqvist J, Ijiri Y, Yamamoto H (2011) Implementation of the Barcelona basic model into TOUGH-FLAC for simulations of the geomechanical behavior of unsaturated soils. Comput Geosci 37(6):751–762

Rutqvist J, Zheng LG, Chen F, Liu HH, Birkholzer J (2014) Modeling of coupled thermo-hydro-mechanical processes with links to geochemistry associated with bentonite-backfilled repository tunnels in clay formations. Rock Mech Rock Eng 47(1):167–186

Sanchez M, Gens A, Guimarães LJDN, Olivella S (2005) A double structure generalized plasticity model for expansive materials. Int J Numer Anal Methods Geomech 29:751–787

Sanchez M, Villar MV, Lloret A, Gens A (2007) Analysis of the expansive clay hydration under low hydraulic gradient. Experiment Unsat Soil Mech 112:309−318

Swartzendruber D (1961) Modification of Darcy's law for the flow of water in soils. Soil Sci 93:22–29

Wang XX, Yang ZM, Sun YP, Liu XX (2011) Experimental and theoretical investigation of nonlinear flow in low permeability reservoir. Procedia Environ Sci 11:1392–1399

Wang YF (2014) Nanogeochemistry: nanostructures, emergent properties and their control on geochemical reactions and mass transfers. Chem Geol 378:1–23

Zeng JH, Cheng SW, Kong X, Guo K, Wang HY (2010) Non-Darcy flow in oil accumulation (oil displacing water) and relative permeability and oil saturation characteristics of low-permeability sandstones. Pet Sci 7(1):20–30

Zou Y (1996) A non-linear permeability relation depending on the activation energy of pore liquid. Geotechnique 46(4):769–774